A Robotic End-Effector for Screwing and Unscrewing Bolts From the Side

Rui Tao, Junfeng Fan, *Member, IEEE*, Fengshui Jing, *Member, IEEE*, Hou Jun, Shiyu Xing, Yunkai Ma, *Graduate Student Member, IEEE*, and Min Tan

***Abstract*—This letter presents a novel robotic end-effector for screwing and unscrewing bolts. In many industrial scenarios, it is required to manipulate bolts from the side using robots with end-effectors. Besides, the reaction torque during tightening needs to be balanced to the stability of the robot. To address these challenges, we design a robotic end-effector that can realize side screwing and torque counteraction. Specifically, through an open gear set and a width-adjustable screwing mouth, the end-effector can approach the bolt from the side in any direction and then screw and unscrew it. A gripper with force-magnification and self-locking drive is equipped to counteract the reaction torque during screwing and unscrewing. Considering the extensions for different application scenarios, a method to extend the end-effector by switching screwing mouths is given, and the extended end-effector is able to screw a variety of objects. After further analysis and optimization of the force and size, experiments are carried out. The results show that the end-effector can screw and unscrew the target bolt robustly and counteract the reaction torque. It is also applicable in different scenarios.**

***Index Terms*—Screwing and unscrewing, grippers and other end-effectors, mechanism design, assembly.**

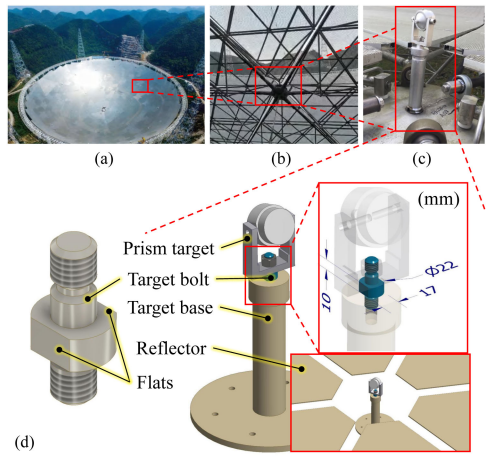

Fig. 1. The prism targets on FAST. (a) Overall view of FAST. (b) The node between the elements. (c) A prism target at a node (d) The structure of the prism target, the target bolt, and the target base.

I. Introduction

SCREWING or unscrewing bolts or nuts from the side is necessary in many industrial scenarios, especially when there are obstacles above bolts. Because few electric wrenches can conduct this operation, at present, it can only be performed manually by workers using entirely mechanical wrenches, which is quite inefficient. In addition, "robots + screwing tools" for automated bolt-tightening is the trend of the future. However, screwing bolts or nuts generates reaction torques, which will be transmitted to the robot and cause the robot to move or even topple if it cannot be fixed properly, such as underwater robots [1], space robots, and mobile robots [2]. Therefore, it is very meaningful to study side screwing and torque counteraction.

The purpose of this study is to automate the work of screwing and unscrewing the target bolts from Five-hundred-meter Aperture Spherical radio Telescope (FAST), which is currently the world's largest single-aperture spherical radio telescope with the highest observation resolution. FAST is mainly composed of an active reflector system and a feed support system. As a part of the measurement and control system, more than 2000 prism targets are deployed on the reflector [3] In the daily maintenance of FAST, replacing the prism targets is very important, and is currently performed manually by workers using wrenches. Manually maintaining the targets is not only inefficient but also extremely dangerous— the reflector is made of aluminum sheets only 1 mm thick and cannot directly bear the weight of a common adult [4]. Therefore, it is necessary to use a light mobile robot to replace human beings for automated target replacement.

Each of the prism targets is assembled on a target base through a target bolt, and the target base is located at the node between the elements of the reflector as shown in Fig. 1. Because the upper and lower threads of the target bolt are in the same direction (Fig. 1(d)), the prism target cannot be driven directly, and only

Manuscript received 13 March 2022; accepted 28 June 2022. Date of publication 20 July 2022; date of current version 29 July 2022. This letter was recommended for publication by Associate Editor Y. Lou and Editor H. Liu upon evaluation of the Reviewers' comments. This work was supported in part by the National Key Research and Development Program of China under Grant 2019YFB1312703, in part by the National Natural Science Foundation of China under Grants 62173327 and 62003341, and in part by the Youth Innovation Promotion Association of CAS under Grant 2022130. *(Corresponding author: Fengshui Jing.)*

The authors are with the State Key Laboratory of Management and Control for Complex Systems, Institute of Automation, Chinese Academy of Sciences, Beijing 100190, China, and also with the School of Artificial Intelligence, University of Chinese Academy of Sciences, Beijing 100049, China (e-mail: taorui2020@ia.ac.cn; fanjunfeng2014@ia.ac.cn; fengshui.jing@ia.ac.cn; houjun2019@ia.ac.cn; xingshiyu2020@ia.ac.cn; mayunkai2019@ia.ac.cn; min.tan@ia.ac.cn).

This letter has supplementary downloadable material available at https://doi.org/10.1109/LRA.2022.3192773, provided by the authors.

Digital Object Identifier 10.1109/LRA.2022.3192773

the target bolt can be driven. Therefore, replacing the prism target is essentially disassembling and assembling the target bolt. Since the target bolt connects the target base and the prism target, it can only be driven through the two flats from the side.

Hence, we design an end-effector that can realize side screwing and torque counteraction. The main components of the end-effector are as follows:

1) A novel screwing mechanism is proposed, which includes an open gear set and a width-adjustable screwing mouth. This design allows the end-effector to screw and unscrew the bolt from the side in any direction. The screwing mechanism can also be used separately to screw various objects by changing the screw mouth.
2) A holding mechanism with force-magnification and self-locking drive is designed to fix the end-effector on the target base during operating, thereby counteracting the reaction torque.
3) A height-adjustable connection is designed to actively adjust the relative position between the screwing mechanism and the holding mechanism.

The design of the end-effector concept throws some new light on side screwing and torque counteraction. The main contributions of this letter are as follows. 1) The idea for side screwing and torque counteraction. 2) The design of a side-screwing mechanism and a gripper with force-magnification and self-locking drive. 3) The optimization of the open gear set and the gripper.

The rest of this paper is organized as follows. Section II introduces the related works. Section III and IV present the design goals and the design of the end-effector, respectively. In Section V, we present the analysis and optimization. Experiments and results are given in Section VI. Finally, conclusions and future work are summarized in Section VII.

II. Related Works

To tighten bolts or nuts, the traditional method is using impact wrenches manually for semiautomated tightening, which is inefficient. Robot assembly technology has been extensively developed [5]. Using robots for thread assembly is the development trend of the future [6] and has already played important roles in many fields [7], such as the assembly of the hubs of wind turbines [8]–[10], the assembly of steel structures in buildings [11], and the maintenance of high voltage lines [12]. In the above research, the basic idea to realize autonomously screwing is "robots + screwing tools," which means that screwing tools are installed at the end of robots as end-effectors.

There are two types of screwing tools: general tools and special tools. Many robotic screwing systems use general screwing tools [13]–[15]. These screwing tools are usually grasped by robots using general parallel grippers, and can even be used manually. Among the general screwing tools, Bosch, Atlas, and other companies launched a series of commercial screwing tools [16], [17].

In addition, researchers have proposed a variety of special screwing tools that can be installed at the end of robots. Müller *et al.* [8] presented a robot-guided tensioning tool for tightening bolts on the hub of the wind turbine. Liu *et al.* [18] proposed an automated bolt tightening shaft that is modularly designed. By a universal joint in the front sleeve, the tool can work normally within a 5 mm deviation. Hu *et al.* [19] developed a screwing tool that can convert linear motion of the parallel gripper into rotational motion. By exchanging tooltips, the tool can screw various bolts. Pei [20] *et al.* developed a mechanical gripper for screwing hexagon socket head bolts. These screwing tools all approach the bolt or nut along the axis and cannot drive the object from the side. Karnati *et al.* [21] designed a robotic hand that can screw and unscrew objects from the side. Due to the complex structure, the maximum screwing torque of the hand is limited, which implies limited application scenarios.

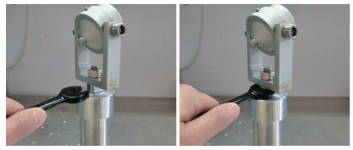

Fig. 2. Manually screw the target bolt. The principle of side screwing is similar to that of manual wrenches.

The casing power tong [22] used in petroleum exploitation provides a design idea for side screwing and inspires us. It is equipped with an open gear set, and the open gear can be driven continuously under the premise of missing teeth. Casing power tongs are heavy equipment and their specific design cannot be directly applied to this letter. Moreover, few researchers have considered balancing the reaction torque of screwing tools.

As these results illustrate, few screwing tools are able to screw and unscrew from the side and counteract the reaction torque. In this work, a robotic end-effector is designed, which is mainly composed of a side-screwing mechanism and a gripper for reaction torque counteraction.

III. Design Goals

The design goals are to achieve side screwing and torque counteraction. The principle of side screwing is shown in Fig. 2. Furthermore, to make the end-effector approach from the side in any direction, the width of the screwing mouth must be adjustable. Because the target base is a cylinder made of steel, we need a mechanism to transfer the reaction torque to the target base. That means a gripper that can hold the cylinder tightly is necessary.

In addition, the compactness of the structure is also very important. Due to the limited space of the node of FAST, we limit the length of the end-effector be less than 220 mm. Taking the above into consideration, the design goals for constructing an end-effector are as follows.

1) The end-effector can screw and unscrew the bolt from the side in any direction. Furthermore, the width of the screwing mouth should be adjustable.
2) The end-effector can hold a cylinder tightly to counteract the reaction torque.
3) The end-effector should have a compact design.

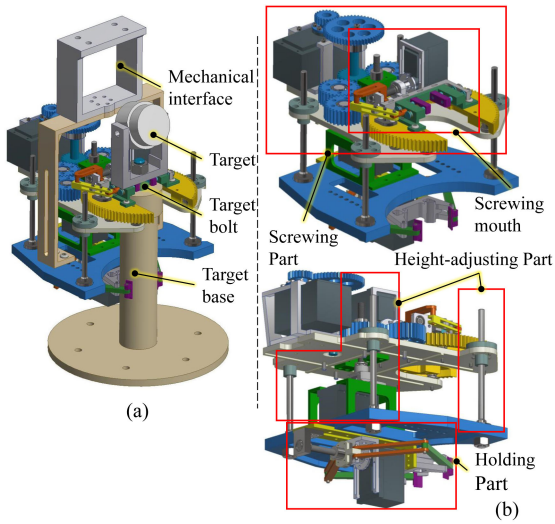

Fig. 3. The structure of the end-effector. (a) The end-effector is fixed on the target base by the Holding Part. (b) Multi-view of the end-effector without the mechanical interface.

IV. Design of the End-Effector

The structure of the end-effector is shown in Fig. 3. The end-effector can be mounted at the end of a robotic arm through a mechanical interface. It can be divided into three parts: a Screwing Part, a Holding Part, and a Height-adjusting Part.

The Screwing Part is mainly composed of an open gear set and a width-adjustable screwing mouth, and it is similar to an adjustable wrench. The Holding Part, essentially a gripper, is to counteract the reaction torque. The end-effector can hold the target base tightly with the gripper. At this point, the torque generated by the Screwing Part is applied to the target base through static friction force rather than transferred to the robotic arm. During screwing or unscrewing, the Holding Part is fixed on the target base, and the Screwing Part moves vertically ($\pm$ *The length of the thread*) with the rotation of the bolt. Therefore, a rigid connection cannot be used directly. The Height-adjusting Part is actually a height-adjustable connection and can adjust the relative position between the Screwing Part and the Holding Part in the vertical direction actively. In the subsections below, we detail the design of the mechanical structure.

A. Screwing Part

1) Transmission Scheme: A gear with several teeth missing, called open gear, is chosen to drive the target bolt from the side. Unlike normal gear sets, an open gear set as shown in Fig. 4 is needed to ensure that the open gear can be driven continuously.

To balance the weight and the output torque of the end-effector, we increase the transmission ratio of the transmission chain and use a low-power motor at the same time. The transmission scheme of the Screwing Part is illustrated in Fig. 4, where a pair of reduction gears are added based on the open gear set.

2) Width-Adjustable Screwing Mouth: A width-adjustable screwing mouth is important for the end-effector to flexibly screw the bolt. As shown in Fig. 5(a), when the screwing mouth is fully open, the end-effector can approach and drive the bolt from the side in any direction. Therefore, the screwing mouth must meet the following two requirements:

- The width is adjustable. The maximum width of the mouth must be larger than the bolts' maximum width.
- To reduce the power of the motor, the transmission chain from the motor to the jaws needs to be self-locking.

The structure of the designed screwing mouth is presented in Fig. 5(b). It is mainly composed of a fixing jaw, two moving jaws, and a driving module. Note that Pin 1, Pin 2, and Pin 3 are used for sliding joints, and Pin 3 is used for a revolute joint. The width of the screwing mouth can be computed by

$$w_2 = 2 \cdot \frac{\theta_{\text{Motor 2}} \cdot p_1}{2\pi} \cdot \frac{b}{a} = \frac{\theta_{\text{Motor 2}} p_1 b}{\pi a}, \tag{1}$$

where w_2 must be larger than the diameter of the middle part of the target bolt. a and b are shown in Fig. 5(c), θ_{Motor2} is the rotation angle of Motor 2, and p_1 is the lead of Lead screw 1. In addition, the force F_{N} shown in Fig. 5(c) will be large when the open gear is tightening the bolt. Therefore, to prevent F_{N} from being transmitted to Motor 2, the designed Lead screw 1 must be self-locking.

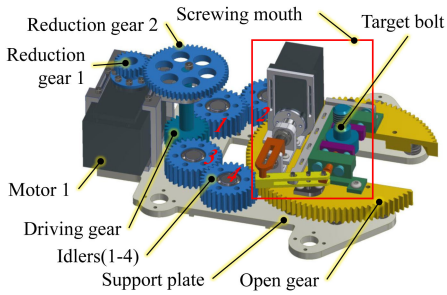

Fig. 4. Transmission chain of the Screwing Part.

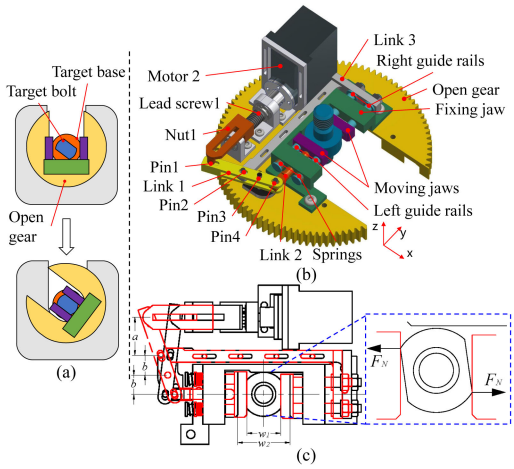

Fig. 5. (a) Alignment process. (b) Structure of the screwing mouth. (c) Schematic diagram of the adjustment process.

B. Holding Part

The design goals of the Holding Part are to design a gripper with a large holding force, light structure, and low energy

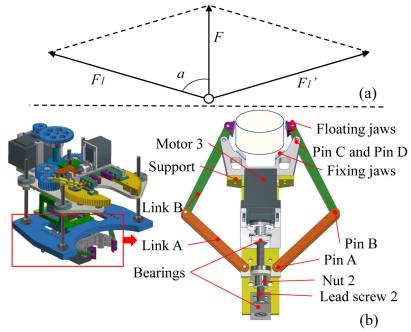

Fig. 6. (a) The principle of the designed force magnification. (b) The structure of the Holding Part.

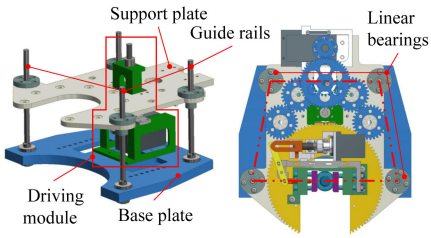

Fig. 7. The structure of the Height-adjusting Part.

cost. Therefore, we must design a force-magnification and self-locking drive. Although there are lots of studies on grippers with large holding force [23]–[25], their sizes and maximum holding forces are both insufficient. The principle of the designed force magnification is shown in Fig. 6(a), where F is the input force and F_1 is the output force. The relationship between F and F_1 is :

$$F_1 = \frac{F}{2\cos\alpha}. \tag{2}$$

To increase the output force F_1, α in (2) should close to 90°, and then $\cos\alpha$ will close to 0. In addition, the thrust F is from a self-locking lead screw, and F_1 further drives a force-magnification lever. The designed structure of the holding gripper is shown in Fig. 6(b). There are four jaws in the Holding Part: two fixing jaws and two floating jaws. When the end-effector reaches the pose to operate, the four jaws will hold the cylinder tightly with the drive of Motor 3. After the holding force is enough, Motor 3 can be powered off. To increase the friction coefficient between the jaws and the target base and prevent slippage, the surfaces of the jaws should be rough, and the curvature radius of the surface of the jaws should be the same as the radius of the target base.

C. Height-Adjusting Part

The structure of the Height-adjusting Part is shown in Fig. 7. Four trapezoidal arranged guide rails are used to constrain the relative position of the Screwing Part and the Holding Part in the horizontal direction, transmit torques, and allow the two to slide in the vertical direction. In the middle of the trapezoid, as shown in Fig. 7, a linear actuator is designed, composed of Motor 4, Nut 3, and Lead screw 3. Nut 3 is fixed on the support plate of the Screwing Part, and Motor 4 is fixed on the base plate, which is connected with the Holding Part. The vertical relative position of the support plate and the base plate can be actively adjusted by the linear actuator.

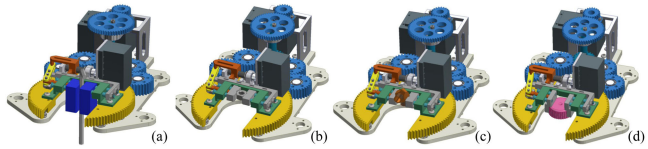

Fig. 8. The extended end-effector with different screwing mouths. (a), (b) are cases to screw common bolts and nuts. An Allen wrench is held by the screwing mouth in (a). (c), (d) are cases to screw special objects that current screwing tools cannot.

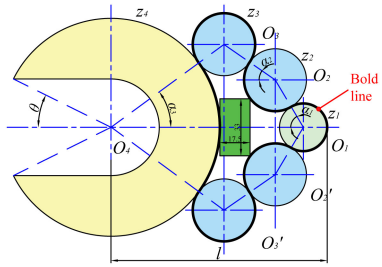

Fig. 9. Installation parameters of the open gear set. For each gear, a part of the reference circle inside or outside the hexagon $O_1O_2O_3O_4O_3'O_2'$ is selected and marked in bold. The bold line marked in the figure represents the curve composed of the bold parts of the reference circles of all the gears.

D. Extensions for Different Application Scenarios

An apparent shortcoming of the above design is that it cannot adapt to more tasks. To extend the application scenarios, we design different shapes of screwing mouths for different tasks, as shown in Fig. 8. The end-effector can be converted to an extended end-effector by changing different screwing mouths. The extended end-effector can not only screw conventional bolts or nuts but also screw objects with complex shapes, such as water pipe joints and bottle caps. The relevant tests will be given in Section VI. B.

V. Analysis and Optimization

This section presents the analysis and the optimization of the Screwing Part and the Holding Part.

A. Optimization of the Gear Arrangement

1) Analysis of the Installation Conditions: To ensure that all gears of the open gear set can mesh correctly, the length of the bold line presented in Fig. 9 must be an integer multiple of the pitch of the gear. As shown in Fig. 9, taking the gear z_2 as an example, the number of patches inside the hexagon $O_1O_2O_3O_4O_3'O_2'$ is:

$$z_{2in} = \frac{\pi - \alpha_1 + \alpha_2}{2\pi} \times z_2. \tag{3}$$

According to the above condition and the geometry constraints of the hexagon, the installation conditions of the open gear set

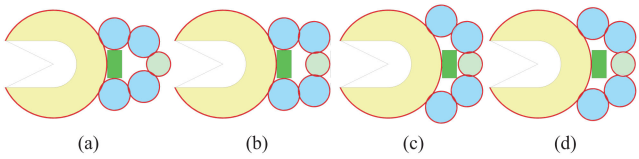

Fig. 10. Different gear arrangements. (a), (b), and (c) represent the optimization process. (d) is the gear arrangement in our implementation.

can be deduced as:

$$z_4\frac{\alpha_3}{\pi}+z_3\frac{\pi+\alpha_3+\alpha_2}{\pi}+z_2\frac{\pi-\alpha_1+\alpha_2}{\pi}+z_1\frac{\pi-\alpha_1}{\pi}=n,$$
$$(z_3+z_4)\sin\alpha_3=(z_2+z_3)\sin\alpha_2+(z_1+z_2)\sin\alpha_1. \quad (4)$$

where α_1, α_2, and α_3 represent the angles of the hexagon, z_1, z_2, z_3 and z_4 are the numbers of teeth of the corresponding gears in Fig. 9.

2) Length Minimization: The goal of the optimization is to minimize the length of the Screwing Part. The dimension parameters shown in Fig. 9 are used for optimization, where l represents the length of the open gear set. Therefore, the optimization goal can be formulated as

$$\min l = 1.25[(z_4+z_3)\cos\alpha_3+(z_3+z_2)\cos\alpha_2 + (z_2+z_1)\cos\alpha_1]. \quad (5)$$

The following geometric constraints are considered.

- The gears must not interfere with other parts. The Height-adjusting Part is represented by a green rectangle, as shown in Fig. 9, which is the closest to the open gear set and needs attention.
- To ensure the open gear can be driven continuously, the angle α_3 must meet $\alpha_3 > \theta$.

To analyze (4), we set the numbers of teeth of the gears to fixed values ($z_1 = 21, z_2 = z_3 = 29, z_4 = 101$) and only care about α_1, α_2, and α_3. The optimization process are as follows. First, Fig. 10(a) shows an gear arrangement where α_3 is at a minimum. Second, to further reduce l, we set the addendum circles of the right three gears tangent to the dashed line as shown in Fig. 10(b), which means α_1 is determined temporarily. At last, increase the value of α_3 with a fixed step until the gears contact the green rectangle as shown in Fig. 10(c). Thus, the interval of α_3 is determined.

For each step of α_3, the corresponding n, α_1, and α_2 cannot be solved directly using (4) because there are more variables than equations. Based on the previous settings, α_1 can be determined temporarily. Therefore, we can compute the corresponding n' and α_2 using (4), and n' is usually an irrational number. Then an approximate integer n is determined from n', for example, $n = 90$ if $n' = 99.235$. n represents the number of the pitches at the bold line and the deviation of the calculation result within 1 is acceptable. Further, By substituting each α_3 and the corresponding n into (4), the corresponding α_2 and α_1 can be calculated.

For each group of α_1, α_2, and α_3, the corresponding l can be computed by (5). Changes of α_2, α_1, and l with respect to α_3 are shown in Fig. 11. When l is minimal, the gears will almost

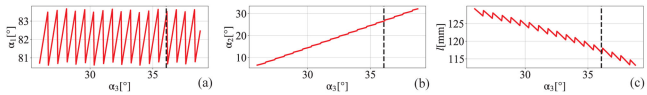

Fig. 11. (a) Changes of α_1 concerning α_3. (b) Changes of α_2 concerning α_3. (c) Changes of l concerning α_3. Black lines are the optimal solution.

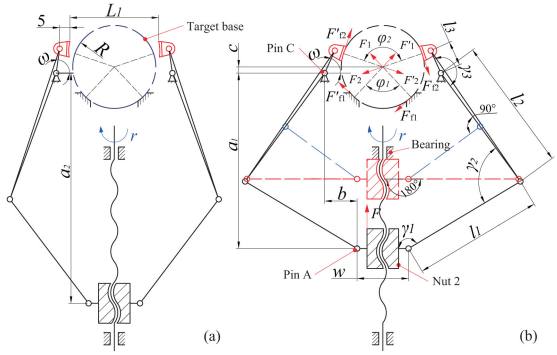

Fig. 12. The schematic diagram of the gripper. (a) The gripper is fully opened. (b) The gripper holds the target base.

contact the green rectangle as shown in Fig. 10(c). For safety reasons, in our implementation, we increase α_3 by about 2° from the minimal value. The optimal values of the angles are as follows: $\alpha_1 = 83.302^\circ$, $\alpha_2 = 26.524^\circ$, and $\alpha_3 = 36.077^\circ$, and the optimal gear arrangement is shown in Fig. 10(d).

B. Optimization of the Holding Part

1) Force Analysis: The relationship between the thrust F of Nut 2 and the force F_2 exerted by the floating jaws on the target base is deduced. The schematic diagram of the gripper is shown in Fig. 12. Based on the geometric relationships, the force F_2 can be computed by

$$F_2=\frac{Fl_2\sin(\gamma_2)}{2l_3\sin(\gamma_1)}=\frac{Fl_2\sin(\omega+\gamma_3-\gamma_1)}{2l_3\sin(\gamma_1)}. \quad (6)$$

where $l_2, l_3, \gamma_1, \gamma_3$ and ω are all marked in Fig 12(b). Among them, ω and γ_3 are not structural parameters, and they can be formulated as

$$\omega=\arccos\frac{l_3}{\sqrt{c^2+(b+\frac{w}{2})^2}}+\arccos\frac{b+\frac{w}{2}}{\sqrt{c^2+(b+\frac{w}{2})^2}}, \quad (7)$$

$$\gamma_1=\arctan\frac{b}{a_1}+\arccos\frac{a_1^2+b^2+l_1^2-l_2^2}{2l_1\sqrt{a_1^2+b^2}}+\frac{\pi}{2}. \quad (8)$$

where a_1 represents the length from Pin C to Pin A when the gripper holds the target base, and can be formulated as

$$a_1=\sqrt{l_1^2-(b-l_2\cos(\omega+\gamma_3))}-l_2\sin(\omega+\gamma_3). \quad (9)$$

It should be noted that the force F_2' from the left floating jaw is equal in magnitude to the force F_2.

2) Size Optimization: The goals of optimization are to make the gripper with a large holding force and compact size. The dimension parameters shown in Fig. 12 are used for optimization.

Geometric Constraints: When the gripper is fully open, the distance L_1 of the two jaws must be larger than the diameter of the target base. Hence, L_1 must meet

$$L_1 \geq 2R + 2, \tag{10}$$

where $R = 26\,\mathrm{mm}$ in our cases. When the gripper holds the target base, a_1 cannot be too small to prevent Nut 2 from contacting the bearing as shown in Fig. 6(b) and Fig. 12(b). In our implementation, a_1 should meet

$$a_1 \geq 84\,\mathrm{mm}. \tag{11}$$

Force Maximization and Length Minimization: The holding force can be computed by (6) – (9). The length of the gripper can be represented by a_2, which is the length from Pin A to Pin C when the gripper is fully opened, as shown in Fig. 12(a).

On the one hand, it can be known from (2) that if γ_1 approaches $180°$, the holding force F will approach infinity. This case is shown in Fig. 12(b) as the red dashed lines. However, in this case, the length of the gripper is large and can be optimized further. On the other hand, making Nut 2 contact the bearing while keeping Link A (l_1) perpendicular to Link B (l_2) can significantly reduce the length. As shown in Fig. 12(b), the blue dashed lines show the case.

To further quantitatively analyze the main force-magnification links, the holding module ($l_3 = 12.5\,\mathrm{mm}$, $c = 3.14\,\mathrm{mm}, b = 16.38\,\mathrm{mm}$) is firstly determined. We set the thrust F to be 4772.8 N by $F = 2\pi\eta T_{\mathrm{Motor1}}/p$, where $T_{\mathrm{Motor1}} = 1\mathrm{N}\cdot\mathrm{m}$, $\eta = 0.95$, and $p = 1.25\,\mathrm{mm}$. Further, we traverse l_1 and l_2 with reference to the interval formed by the red and blue dashed lines. And the changes of F_2 and a_1 with respect to l_1 and l_2 can be obtained. The value of w in (7) is $26\mathrm{mm}$ and it is determined by the width of a commercial nut – Nut 2. When the gripper is fully opened, the length a_2 can also be computed by (9) like a_1, where ω cannot be calculated by (7), but by

$$\omega = \frac{2b + w - L_1 - 10}{2l_3}, \tag{12}$$

where $L_1 = 2R + 2$, $R = 21\,\mathrm{mm}$. When Link B is a straight link ($\gamma_3 = 180°$), F_2, a_1, and a_2 change with respect to l_1 and l_2 are respectively shown in Fig. 12 (b.1), (b.2), and (b.3). To further discuss how the shape of the links influences the results, γ_3 is changed. We decrease and increase γ_3 by $6°$, and the corresponding results are shown in Fig. 12(a) and (b), respectively.

According to the results in Fig. 13, the trends of the three rows are almost the same. That is to say, to get a maximum holding force, we must make l_1 be as small as possible and l_2 be as large as possible. To get a minimum length, the l_1 and l_2 should be both as small as possible. However, when we choose the former, compared to the latter, the increase in length a_2 is not very drastic, but the holding force F is greatly increased. Hence, a large l_1 and a small l_2 are the best solution. Furthermore, under the premise of $a_1 \geq 84\,\mathrm{mm}$, when $\gamma_3 = 174°$, the corresponding a_2 is the smallest and F_2 is the largest among the three rows.

In practice, the holding force of the gripper comes from the elastic force generated by the elastic deformation of the links, as

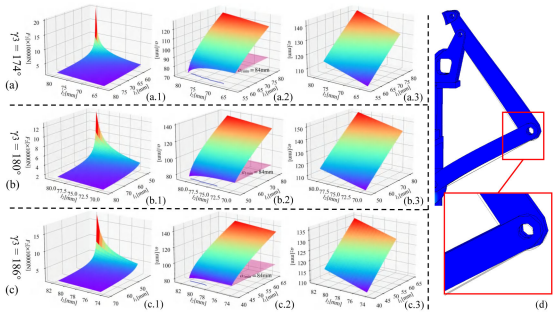

Fig. 13. (a), (b), (c) When $\gamma = 174°$, $\gamma = 180°$, and $\gamma = 186°$, changes of F_2, a_1, and a_2 with respect to l_1 and l_2. The planes in (a.2), (b.2), and (c.2) are the boundaries of a_1. The intersections of the colorful surfaces and the planes form curves, which are projected on the XY planes as the blue curves. (d) The elastic deformation of the links. The black lines represent the original shape without deformation.

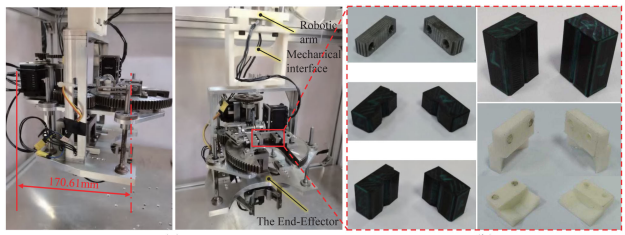

(a) (b)

Fig. 14. (a) The prototype of the end-effector. (b) Various screwing mouths.

presented in Fig. 13(d). To make the links elastically deform, Nut 2 should be moved towards the motor for a short distance after the floating jaws contact the target base. Therefore, a_1 should be slightly larger than 84 mm. We will discuss this further in Section VI. C. In our implementation, γ_3 is chose to be $174°$, $l_1 = 68\,\mathrm{mm}$ and $l_2 = 76\,\mathrm{mm}$. Note that γ_3 can be chosen to be smaller than $174°$, and interested readers can deduce it further.

VI. Experiments and Results

We prototyped the end-effector as shown in Fig. 14(a). To ensure the stiffness of the end-effector, the main parts were made of carbon steel and aluminum, and the others that are not important, such as the mechanical interface, are made of photosensitive resin. The total weight is about 4.6 kg, and the maximum length from the open gear's axis to the back is 170.61 mm as shown in (a). To extend the use of the end-effector, we made various screwing mouths, as shown in Fig 14(b). Next, we will first test the Screwing Part and the Holding Part separately, and then test the workflow of the end-effector.

A. Test of the Screwing Part

The Screwing Part was removed from the end-effector and mounted on the end of a 6-DOF robotic arm through a new mechanical interface, as shown in Fig. 15(b). Fig. 15 (c.1–c.4) shows the process of screwing and unscrewing the target bolt. The Screwing Part approaches the target bolt from the side. After reaching the target pose, the open gear rotates to the target

Fig. 15. (a.1) The target bolts. (a.2,3) Hexagon bolts or nuts. (a.4,5) Irregularly shaped objects like pipe joints and special bolts. (a.6) Common bolts. (a.7) Cylinders like bottle caps. (b) The Screwing Part was mounted at the end of a 6-DOF robotic arm. (c.1) Approaching the target bolt. (c.2) Reaching the target pose. (c.3) Adjusting the direction and width of the screwing mouth. (c.4) Screwing and unscrewing. (d.1-6) Screwing objects that are shown in (a.2-7).

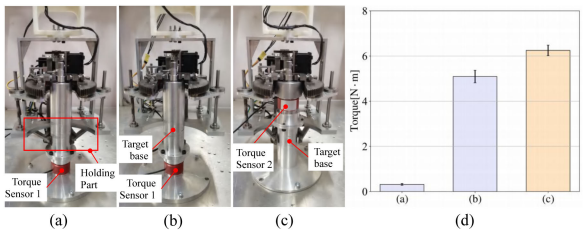

Fig. 16. (a), (b), (c) Experimental settings for measuring the external reaction torque with the Holding Part, the external reaction torque without the Holding Part, and the internal reaction torque with the Holding Part. (d) Means and standard deviations of the torques in (a), (b), and (c).

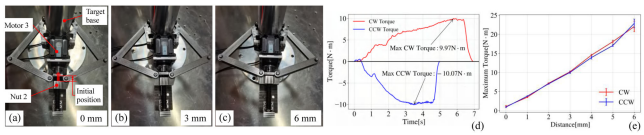

Fig. 17. (a), (b), (c) Holding Part holds the target base when Nut 2 is at different position. (d) Typical changes of the applied torques when the position of Nut 2 is 3 mm moved. (e) Changes of the maximum torque with respect to the moved distance.

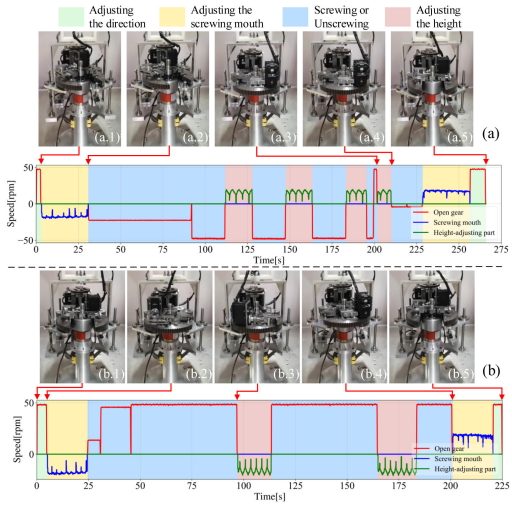

Fig. 18. Changes of the speeds of the three motors. (a) is the screwing process. (b) is the unscrewing process. The key time instants and their corresponding time stamps are shown in the figure.

direction, and the width of the screwing mouth is adjusted. Then the target bolt can be screwed or unscrewed.

To test the performance of the extended end-effector with various screwing mouths as mentioned in Section. IV. D, we conducted experiments to screw hexagon bolts and nuts as shown in Fig. 15 (a.2) and (a.3), irregularly shaped objects as shown in (a.4) and (a.5), cylinders like bottle caps as shown in (a.6), as well as using an Allen wrench to screw a common bolt as shown in (a.7). The results are shown in (d.1-6). All the objects mentioned above can be successfully screwed repeatedly.

B. Test of the Holding Part

The Holding Part was evaluated from two aspects: the effectiveness of torque counteraction and the maximum holding torque of the gripper. First, to test the effectiveness of the Holding Part, we performed experiments as shown in Fig. 16(a)-(c). Fig. 16(a) and (b) show the end-effector with the Holding Part and without the Holding Part, respectively. Torque Sensor 1 is located between the target base and the ground to measure the external reaction torque. Torque Sensor 2 is embedded in the target base with a location between the Screwing Part and the Holding Part to measure the internal reaction torque. We programmed the end-effector to tighten the target bolt with a target torque of 6 $\mathrm{N \cdot m}$ (using current and angle feedback) and repeated it 15 times with the settings in (a), (b), and (c), respectively. Fig. 16(d) shows the results. The analyses are as follows. 1) Compared to the mean of the reaction torque in (c), that in (a) is quite small. The result proves that the Holding Part can definitely counteract the reaction torque. 2) The mean of the external reaction torque in (b) is smaller than that in (c), which is caused by the deformation of the mechanical interface in (b). This result demonstrates that when screwing bolts without torque counteraction, The stiffness of the mechanical interface must be high and the robot should be well fixed, otherwise, the tightening torque cannot be guaranteed.

Second, the maximum holding torque of the gripper was tested. As shown in Fig. 17 (a-c), the gripper was evaluated separately. The surfaces of the floating jaws and fixing jaws were roughened to increase the friction coefficient. The gripper was driven by Dynamixel AX-12 A motor, which has a stall torque of 1.5 $\mathrm{N \cdot m}$. As mentioned in Section V. B, the holding force is related to the position of Nut 2. To test the relationships between them, we moved Nut 2 towards Motor 3 in 1 mm steps from an initial position. The initial position is the position of Nut 2 when the floating jaws just contact the target base, as shown in Fig. 17(a). In each step, we de-energized the motor after the gripper held the target base, and then a clockwise (CW, for screwing) or counterclockwise (CCW, for unscrewing) force was slowly and increasingly applied to the gripper until slippage occurs. The torque caused by the applied force can be recorded by the torque sensor between the target base and the ground. Typical changes of the torques are shown in Fig. 17(d). It can be seen that when slippage occurs, the recorded torque will not increase but decrease a little. Therefore, we can roughly regard the peak of each test as the maximum holding torque. After slipping for about 1 s, the force was removed, so the recorded

torque dropped suddenly. We repeated the operation 15 times in each step, and the results are shown in Fig. 17(e). The maximum holding torque increases nearly linearly with the movement of Nut 2. When Nut 2 is 6 mm moved from the initial position, the maximum holding torque is about 22-23 $\mathrm{N \cdot m}$, which can ensure that the end-effector does not slip when tightening the target bolt.

C. Test of the Workflow of the End-Effector

We programmed the end-effector to approach the target bolt from the side and then screw and unscrew it. After reaching the target pose, the Holding Part held the target base, and the rotational speeds of the three motors that respectively drive the open gear, the screwing mouth, and the Height-adjusting Part were recorded. The results are shown in Fig. 18. We repeated the experiment 10 times and the end-effector can successfully and robustly screw and unscrew the target bolt without failure.

VII. Conclusions and Future Work

In this letter, an end-effector for screwing and unscrewing the target bolt was designed. The end-effector could approach the bolt from the side in any direction, automatically screw and unscrew it, and counteract the reaction torque. An open gear set and a width-adjustable screwing mouth were designed for side screwing. A gripper driven by a small-power motor could obtain a great holding force because of the force-magnification and self-locking design. We also gave some extensions of the end-effector to perform more tasks. Analysis and optimization were carried out to make the end-effector compact and with a large holding force. Experiments showed that a prototype of the end-effector could screw and unscrew the target bolt from the side robustly and almost completely counteract the reaction torque. The extended end-effector could screw various objects that traditional tools cannot.

The design concept can be applied to many industrial scenarios. In actual use, if the torque counteraction function is needed, the limitation of the end-effector is that the threaded hole must be at the center of a raised base, such as a cylinder, and the shapes of the jaws should be refined to suit the base. If the function is not needed, compared with traditional wrenches, the screwing method proposed in this letter can screw more kinds of objects and may be more advantageous in the scenario where there are obstacles above the object. However, in the present design, we did not consider the cable twist problem for Motor 2 (the motor for the screwing mouth). We will improve it using slip rings [26] in the next generation.

In the future, we will further optimize the design and develop intelligent algorithms for screwing various objects.

References

[1] Y. Wang, S. Wang, Q. Wei, M. Tan, C. Zhou, and J. Yu, "Development of an underwater manipulator and its free-floating autonomous operation," *IEEE/ASME Trans. Mechatron.*, vol. 21, no. 2, pp. 815–824, Apr. 2016.

[2] Y. Wu, P. Balatti, M. Lorenzini, F. Zhao, W. Kim, and A. Ajoudani, "A teleoperation interface for loco-manipulation control of mobile collaborative robotic assistant," *IEEE Robot. Autom. Lett.*, vol. 4, no. 4, pp. 3593–3600, Oct. 2019.

[3] R. Nan et al., "The five-hundred-meter aperture spherical radio telescope (FAST) project," *Int. J. Mod. Phys. D.*, vol. 20, no. 06, pp. 989–1024, 2011.

[4] R. Nan, "Five hundred meter aperture spherical radio telescope (FAST)," *Sci. China. Ser. G.*, vol. 49, no. 2, pp. 129–148, 2006.

[5] R. Li and H. Qiao, "A survey of methods and strategies for high-precision robotic grasping and assembly tasks—some new trends," *IEEE/ASME Trans. Mechatron.*, vol. 24, no. 6, pp. 2718–2732, Dec. 2019.

[6] A. Salem and Y. Karayiannidis, "Robotic assembly of rounded parts with and without threads," *IEEE Robot. Autom. Lett.*, vol. 5, no. 2, pp. 2467–2474, Apr. 2020.

[7] C. Ding, L. Lu, C. Wang, and C. Ding, "Design, sensing, and control of a novel UAV platform for aerial drilling and screwing," *IEEE Robot. Autom. Lett.*, vol. 6, no. 2, pp. 3176–3183, Apr. 2021.

[8] R. Müller, M. Vette, and L. Hörauf, "An adaptive and automated bolt tensioning system for the pitch bearing assembly of wind turbines," *Robot. Comput.-Integr. Manuf.*, vol. 36, pp. 119–126, 2015.

[9] E. L. Secco, A. Nagar, C. Deters, H. Wurdemann, H.-K. Lam, and K. Althoefer, "A neural network clamping force model for bolt tightening of wind turbine hubs," in *Proc. IEEE Int. Conf. Comput. Inf. Technol*., 2015, pp. 288–296.

[10] C. Deters, H.-K. Lam, E. L. Secco, H. A. Würdemann, L. D. Seneviratne, and K. Althoefer, "Accurate bolt tightening using model-free fuzzy control for wind turbine hub bearing assembly," *IEEE Trans. Control Syst. Technol.*, vol. 23, no. 1, pp. 1–12, Jan. 2015.

[11] B. Chu, K. Jung, K. H. Ko, and D. Hong, "Mechanism and analysis of a robotic bolting device for steel beam assembly," in *Proc. IEEE Int. Conf. Control Autom. Syst.*, 2010, pp. 2351–2356.

[12] E. Tani, H. Yamada, R. Kato, K. Kurabe, K. Yamashita, and K. Tatsuno, "Development of the tightening nut task skill using a power distribution line maintenance experimental robot," in *Proc. IEEE/SICE Int. Symp. Syst. Integr.*, 2015, pp. 558–563.

[13] T. Murooka, K. Okada, and M. Inaba, "Self-repair and self-extension by tightening screws based on precise calculation of screw pose of self-body with cad data and graph search with regrasping a driver," in *Proc. IEEE-RAS Int. Conf. Humanoid Robots*, 2019, pp. 79–84.

[14] K. Pfeiffer, A. Escande, and A. Kheddar, "Nut fastening with a humanoid robot," in *Proc. IEEE/RSJ Int. Conf. Intell. Robots Syst*., 2017, pp. 6142–6148.

[15] F. V. Drigalski, C. Nakashima, Y. Shibata, Y. Konishi, and K. Harada, "Team o2as at the world robot summit 2018: An approach to robotic kitting and assembly tasks using general purpose grippers and tools," *Adv. Robot.*, vol. 34, no. 78, pp. 514–530, 2020.

[16] Cordless impact wrenches, 2020. [Online]. Available: https://www.boschtools.com/us/en/boschtools-ocs/cordless-impact-wrenches-37651-c/

[17] Atlas - continuous rotation, 2022. [Online]. Available: https://www.atlascopco.com/en-us/itba/products/bolt-tightening-solutions/continuous-rotation

[18] S. Liu, S. S. Ge, and Z. Tang, "A modular designed bolt tightening shaft based on adaptive fuzzy backstepping control," *Int. J. Control Autom. Syst.*, vol. 14, no. 4, pp. 924–938, 2016.

[19] Z. Hu, W. Wan, K. Koyama, and K. Harada, "A mechanical screwing tool for parallel grippers—Design, optimization, and manipulation policies," *IEEE Trans. Robot.*, vol. 38, no. 2, pp. 1139–1159, Apr. 2022.

[20] M. Pei, K. Xu, X. Ding, S. Jiang, and X. Gao, "Design and analysis of continuous rotating multifunctional mechanical gripper," in *Proc. IEEE Int. Conf. Robot. Biomimetics*, 2018, pp. 2007–2012.

[21] N. Karnati, B. A. Kent, and E. D. Engeberg, "Bioinspired sinusoidal finger joint synergies for a dexterous robotic hand to screw and unscrew objects with different diameters," *IEEE/ASME Trans. Mechatron.*, vol. 18, no. 2, pp. 612–623, Apr. 2013.

[22] X. Cao, M. f. huang, J. Liu, and Z. Wei, "Discuss for design of notched gear driive unit," *OIL FIELD EQUIPMENT*, vol. 32, no. 6, pp. 37–39, 2003.

[23] T. Takayama, T. Yamana, and T. Omata, "Three-fingered eight-DOF hand that exerts 100-N grasping force with force-magnification drive," *IEEE/ASME Trans. Mechatron.*, vol. 17, no. 2, pp. 218–227, Apr. 2012.

[24] W. Zuo, G. Song, and Z. Chen, "Grasping force control of robotic gripper with high stiffness," *IEEE/ASME Trans. Mechatron*., vol. 27, no. 2, pp. 1105–1116, Apr. 2022.

[25] Y. Su et al., "A high-payload proprioceptive hybrid robotic gripper with soft origamic actuators," *IEEE Robot. Autom. Lett.*, vol. 5, no. 2, pp. 3003–3010, Apr. 2020.

[26] M. Tennomi et al., "Development of assembly system with quick and low-cost installation," *Adv. Robot.*, vol. 34, no. 78, pp. 531–545, 2020.